Statistical Connection between the Madden–Julian Oscillation and Large Daily Precipitation Events in West Africa

AWOLOU SOSSA,[a,b] BRANT LIEBMANN,[c,d] ILEANA BLADÉ,[e] DAVE ALLURED,[c,d] HARRY H. HENDON,[f] PETE PETERSON,[g] AND ANDREW HOELL[d]

[a] *Significant Opportunities in Atmospheric Research and Science, UCAR, Boulder, Colorado*
[b] *Department of Civil Engineering, The City College of New York, New York, New York*
[c] *CIRES, University of Colorado, Boulder, Colorado*
[d] *Physical Sciences Division, NOAA/Earth System Research Laboratory, Boulder, Colorado*
[e] *Secció de Meteorologia, Department de Fisica Aplicada, Universitat de Barcelona, Barcelona, Spain*
[f] *Bureau of Meteorology Research Centre, Melbourne, Victoria, Australia*
[g] *Climate Hazards Group, Department of Geography, University of California, Santa Barbara, Santa Barbara, California*

(Manuscript received 16 February 2016, in final form 4 December 2016)

ABSTRACT

This study focuses on the impact of the Madden–Julian oscillation (MJO)—as monitored by a well-known multivariate index—on large daily precipitation events in West Africa for the period 1981–2014. Two seasons are considered: the near-equatorial wet season in March–May (MAM) and the peak of the West African monsoon during July–September (JAS), when the intertropical convergence zone (ITCZ) is at its most northerly position. Although the MJO-related interannual variation of seasonal mean rainfall is large, the focus here is on the impacts of the MJO on daily time scales because variations in the frequency of intense, short-term, flood-causing, rainfall events are more important for West African agriculture than variations in seasonal precipitation, particularly near the Guinean coast, where precipitation is abundant. Using composites based on thresholds of daily precipitation amounts, changes in mean precipitation and frequency of the heaviest daily events associated with the phase of the MJO are investigated. The expected modulation of mean rainfall by the MJO is much stronger during MAM than during JAS; yet the modulation of the largest events (i.e., daily rainfall rates above the 90th percentile) is comparable in both seasons. Conservative statistical tests of local and field significance indicate unambiguous impacts of the MJO of the expected sign during certain phases, but the nature of the impact depends on the local seasonal precipitation regime. For instance, in JAS, the early stages of the MJO increase the risk of flooding in the Sahel monsoon region while providing relief to the dry southern coast.

1. Introduction

West Africa as defined in this study is located within 3°–19°N, 18°W–11°E, extending from the Gulf of Guinea to the Sahara Desert, and is home to more than 300 million people. Agriculture is the dominant industry, employing around half of the active population. Since irrigation is not well developed, rainfall is the primary control on crop production. Both a deficit and an overabundance of rainfall can lead to crop reductions, which threaten food security if severe. In the north, including the Sahel semiarid region, an area that suffers from periodic droughts (Rodríguez-Fonseca et al. 2015), a lack of rainfall is often (but not always) the more serious issue. In the wetter climates to the south, however, excess rainfall is usually the problem. In particular, short-term excess amounts cause local flooding, resulting in crop failure and infrastructure damage as the soil becomes saturated, because dams and other water retention structures are rare.

The Madden–Julian oscillation (MJO; also referred to as the 40–50- or 30–60-day oscillation) is a large-scale tropical disturbance that originates over the Indian Ocean and propagates eastward, occasionally circumnavigating the equator (Madden and Julian 1971, 1972). Despite its intermittent nature, with active periods followed by quiescence (e.g., Matthews 2004), the MJO constitutes the primary coherent mode of intraseasonal variability (roughly defined as fluctuations with periods between 20 and 90 days) in the tropics (Madden and Julian 1994). Its

Corresponding author e-mail: Brant Liebmann, brant.liebmann@noaa.gov

DOI: 10.1175/JCLI-D-16-0144.1

most prominent characteristic is a convective center that appears to spontaneously develop over the Indian Ocean and thereafter progresses eastward, although Straub (2013) has argued that the initiation of Indian Ocean convection is sometimes preceded by slow, eastward-moving wind anomalies over eastern Africa. The convection propagates eastward at about 5 m s^{-1}, has a zonal wavenumber-2 scale confined to the Eastern Hemisphere and has been interpreted as a Rossby–Kelvin wave convectively coupled via frictional moisture convergence (Hendon and Salby 1994; Lau et al. 2012). As the convection dies off near the date line, the now uncoupled and dry Kelvin-like disturbance continues eastward at about 10 m s^{-1} (Hendon and Salby 1994), eventually reaching West Africa, having completed almost a full circle around the globe.

One may then expect the MJO to have little impact on West Africa, and indeed the first studies reported only modest precipitation anomalies—and only in northern summer—occurring concomitantly with the development of convection over the equatorial Indian Ocean (Knutson and Weickmann 1987; Annamalai and Slingo 2001). Later studies have shown the existence of both positive and negative precipitation anomalies in West Africa coherent with the MJO (e.g., Matthews 2004; Wheeler and Hendon 2004), but ones that should not be viewed as mere extensions of the Indian Ocean anomalies. For instance, the positive convective signal arises a few days before the onset of convection over the Indian Ocean (Wheeler and Hendon 2004), it tends to propagate westward (Janicot et al. 2009), and its strength is unrelated to the intensity of convection over the warm pool (Pohl et al. 2009). These last authors also report that the West Africa dry anomalies that arise during dry MJO phases in the Indian Ocean tend to be stronger and more coherent than those seen during wet phases.

Matthews (2004) has argued that the MJO-related convection over West Africa is triggered when the dry eastward-propagating Kelvin wave meets with a westward-propagating Rossby wave emanating from the same region of reduced convection in the warm pool, forcing deep ascent and midtropospheric cooling, thus destabilizing the troposphere over West Africa. The time required for the two wave fronts to meet is about 20 days. Maloney and Shaman (2008) confirmed that the MJO modulates 30–90-day precipitation variability in this region, and Gu (2009) found a strong spectral peak in precipitation at 30–80-day time scales during the March–June season confined mainly to the Guinean coast, which was also attributed to the MJO.

In addition to strongly modulating precipitation over West Africa, the MJO may influence short-term large rainfall events, as it does in other regions. For instance, Wheeler and Hendon (2004) reported a tripling of weekly upper-quintile rainfall in northern Australia during wet compared to dry MJO phases. On a global basis, Jones et al. (2004b) found that, in regions with a statistically significant intraseasonal MJO signal, the number of pentad extremes is increased by 40% during active compared to quiescent periods. Over Africa, Berhane et al. (2015) found, upon averaging over a large region that included the Guinea coast, large changes in the distribution of daily rainfall amounts, depending on whether convection over West Africa was enhanced or suppressed by the MJO. However, the spatial distribution of these changes was not examined. Since large short-term precipitation events can be of concern in West Africa, it would be of great interest to assess in more detail to what extent the frequency of occurrence of the largest daily precipitation events may be increased or decreased by the presence of the MJO and how this influence varies depending on the local seasonal precipitation regime (i.e., locally wet or locally dry monsoon season). Although the interaction between the West African monsoon and the MJO is beyond the scope of this paper, we believe our results could provide an interesting lead for dynamical studies of such interaction.

The present study thus documents and analyzes in detail the spatial changes in the frequency of the largest daily precipitation events in West Africa related to variations in the MJO. We focus on two distinct seasons: March–May (MAM), when the intertropical convergence zone (ITCZ) and maximum mean rainfall are near the equator, and July–September (JAS), at the peak of the West African monsoon and when the ITCZ is at its most northerly position. Local and field statistical significance of enhancement and reduction in the frequency of the largest daily events are estimated conservatively using randomization methods.

While it is important to document the spatial variation of large precipitation events connected to the MJO, the ultimate practical benefit of understanding how the MJO modulates the heaviest events in West Africa is that it would provide a basis for predicting the probability of occurrence of such events by capitalizing on the known potential skill of forecasts of intraseasonal MJO anomalies up to 20 days in advance (e.g., Jones et al. 2004a). This, in turn, would allow for better flash-flood management and emergency response planning.

2. Data

Precipitation over Africa is estimated using the Climate Hazards Group Infrared Precipitation with Station data (CHIRPS; Funk et al. 2014). This product is a blend of Climate Hazards Group precipitation climatology (Funk et al. 2015), satellite infrared measurements, and

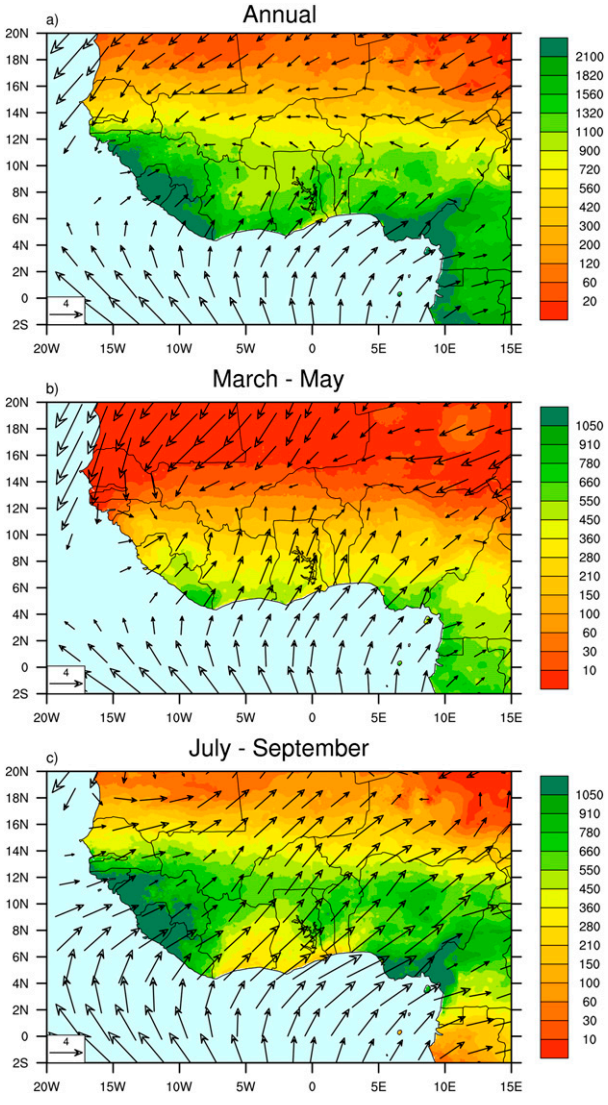

FIG. 1. Average precipitation total (mm) and 925-hPa wind for (a) annual, (b) MAM, and (c) JAS for 1981–2014. Note the uneven shading intervals and the factor-of-2 difference between annual and seasonal totals. Reference wind vector ($m\,s^{-1}$) is shown in the bottom-left corner. Wind vectors are plotted at every third grid point, and those with amplitudes less than $1\,m\,s^{-1}$ are omitted.

direct rain gauge measurements (which are sparse over West Africa). This study employs the 0.25° version for the period 1981–2014. Berhane et al. (2015) performed their analyses using both CHIRPS and Global Precipitation Climatology Project (Huffman and Bolvin 2013) daily precipitation and obtained consistent enough results that they deemed it not necessary to include results from both datasets in their paper.

The winds are from the European Centre for Medium-Range Weather Forecasts interim reanalysis (ERA-Interim; ECMWF 2009), represented on a 0.7° grid. Satellite-based outgoing longwave radiation (OLR) measurements are used to depict areas of large-scale convection and subsidence in the tropics.

3. Results

Figure 1a shows average annual precipitation for an extended West African domain. There is a sharp meridional gradient from $50\,mm\,yr^{-1}$ north of the Sahel semiarid region (located roughly between 12° and 18°N) southward toward the coast and southeastward toward the western Congo basin, where values exceed $2\,m\,yr^{-1}$ in some of the coastal regions. The seasonality of precipitation is pronounced in West Africa, associated with the meridional movement of the ITCZ, which, at its northernmost extent, during northern summer, is centered near 10°N (Sultan and Janicot 2003). Because this study is concerned with the MJO impact on large daily precipitation events, it focuses on two relatively wet seasons, MAM and JAS, for which climatological total amounts are shown in Figs. 1b and 1c.

MAM (Fig. 1b) is an important wet season along the south coast and also encompasses the end of the wet season in the Congo basin. The Sahel is still dry at that time, consistent with Sultan and Janicot (2003), who consider May and June to be the ''premonsoon'' season for Sahelian West Africa (west of 30°E and north of the equator). The largest amounts of rainfall are found near the Guinean coast, with a uniform decrease in precipitation with latitude. Weak low-level southerlies are evident in the southern half of the domain, extending into the zone of large meridional precipitation gradients, at about 12°N, where there is convergence with northerlies. The southerlies advect moisture into this region from the Gulf of Guinea (Sultan and Janicot 2003).

JAS (Fig. 1c) is quite different. In general, there is more precipitation than in MAM, as the ITCZ has moved northward from the equator. There are substantial zonal variations compared to MAM, especially south of the Sahel, where more than 1 m falls in the far west but much less precipitation occurs in the east. Moreover, the coastal region from about 8°W to 4°E is dry compared to the surrounding longitudes and actually drier than in MAM. Southwesterly flow, stronger than in MAM, now extends through the entire domain. These southwesterlies efficiently transport oceanic moisture into the western Sahel (Pu and Cook 2010), flowing perpendicular to the coast and Guinea Highlands and yielding the largest West African JAS rainfall in that season.

The transition between these two seasons is not smooth, but rather occurs as a ''monsoon jump'' in late June during which the belt of heaviest precipitation abruptly shifts from 5° to 10°N (Sultan and Janicot 2000; Le Barbé et al. 2002; Sultan and Janicot 2003). Several hypotheses

have been proposed to explain this abrupt June transition, invoking mechanisms that entail the buildup and release of instability on various scales (Sultan and Janicot 2003; Hagos and Cook 2007).

An index for monitoring the MJO developed by Wheeler and Hendon (2004) has been used for the current study. This index [also referred to as the Real-Time Multivariate MJO (RMM) index] is constructed from daily anomalies of OLR and zonal wind at 850 and 200 hPa, both averaged from 15°N to 15°S, subjected to a combined empirical orthogonal function (EOF) analysis using a covariance matrix (prior to the analysis, each field is normalized by its global variance). The first two EOFs explain similar amounts of variance but are well separated from the third. As they are in quadrature and quite coherent in the 30–80-day band (with an average coherence of 0.76), they represent a propagating mode. Eight phases are then defined, depending on the signs of the two principal component time series, with the MJO considered globally weak or inactive when the combined normalized amplitude is less than 1.25. This yields 1575 (50.4%) inactive days in MAM and 1946 (62.2%) in JAS for the 1981–2014 period. The distribution of active days that fall in each phase can be quite different in the two seasons: for example, phase 8 has more than twice as many days in MAM (227) as in JAS (96).

The RMM index usually, but not always (Straub 2013), gives similar results to those obtained using the indices developed by Kiladis et al. (2014), which uses OLR only, and Jones et al. (2015), which is identical to the RMM index except for a 20–90-day bandpass filtering. Since the RMM index does not entail filtering in time, it is well suited for the ultimate goal of this paper, which is to improve forecasting of large daily precipitation events in Sahelian West Africa.

One caveat of using the RMM index is that there is no guarantee that a large daily value of the index always indicates the presence of an MJO event. For example, an organized mesoscale convective complex might project onto one of the EOFs and yet not be related to the MJO. As a test, additional criteria were added to the amplitude condition and "active MJO days" were defined only if the index was also consistent with the expected MJO phase progression over 3-day sequences (e.g., phase 5 should be followed by phase 6). On average, 6 days were lost per phase, or about 3.6% of the original days, with otherwise nearly identical results.

Figure 2 shows composites of global tropical OLR anomalies based on the MJO phase, as determined by the RMM index. The panels display the composite for the days in each phase minus the composite for all days in the inactive phase. Although the EOFs have been determined from annual data, the results are stratified by season: MAM (Fig. 2, left) and JAS (Fig. 2, right). Consistent with Wheeler and Hendon (2004), the composites show the development and slow eastward propagation of the main convective signal from the Indian Ocean to just west of the date line. The general pattern is the same in both seasons, but the main centers of action are wider, stronger, and more centered along the equator and exhibit a clearer eastward propagation in MAM than JAS. The more pronounced character of the MJO anomalies in MAM is particularly evident over West Africa. There, moderate negative OLR anomalies (indicating enhanced convection) are present in MAM during phases 8, 1, and to a lesser extent phase 2, while in phases 4 and 5 positive OLR anomalies (suppressed rainfall) prevail. In contrast, only weak anomalies can be seen in JAS. In phase 7, West African OLR anomalies are negative in MAM (Fig. 2g) but weakly positive in JAS (Fig. 2o).

Upper-level zonal wind anomalies are also shown in Fig. 2. In MAM, as the convective anomaly develops over the Indian Ocean (phase 1), easterlies appear to the west and westerlies to the east, consistent with upper-level outflow. The easterly winds extend over West Africa in phases 2 and 3 (Figs. 2b,c) but are strongest at the equator. They then weaken at the equator but remain easterly over West Africa during phase 4 (Fig. 2d), while the local OLR anomalies become positive. At the same time, upper-level westerlies appear over the eastern Pacific. They seem to originate as outflow east of the main MJO convective center and propagate rapidly eastward, with maximum amplitude on the equator, which is consistent with the uncoupled dry Kelvin wave response described by Hendon and Salby (1994), and reach Africa by phase 5 (Fig. 2e). Winds remain westerly over West Africa during the next three phases. In JAS (Fig. 2, right), the wind anomalies are weaker than in MAM but otherwise similar, particularly in the Western Hemisphere.

We now turn our attention to the possible impact of the MJO on the largest daily precipitation events. While we expect a general correspondence between OLR and increased extremes, precipitation influenced by local instabilities or small-scale orography may not be reflected in the large-scale OLR fields. For the present study, those daily amounts that equal or exceed the 90th percentile of all daily amounts (including zeros) for a given season are analyzed and are hereinafter referred to as "heavy" precipitation events. These 90th-percentile values for West Africa are shown for MAM in Fig. 3a. As expected, the threshold patterns line up closely with seasonal mean precipitation and do not vary qualitatively when this percentile is changed. The largest values are found along the coast and decrease uniformly with latitude. North of 15°N there is virtually no precipitation (Fig. 1a) and fewer than 10% of days record

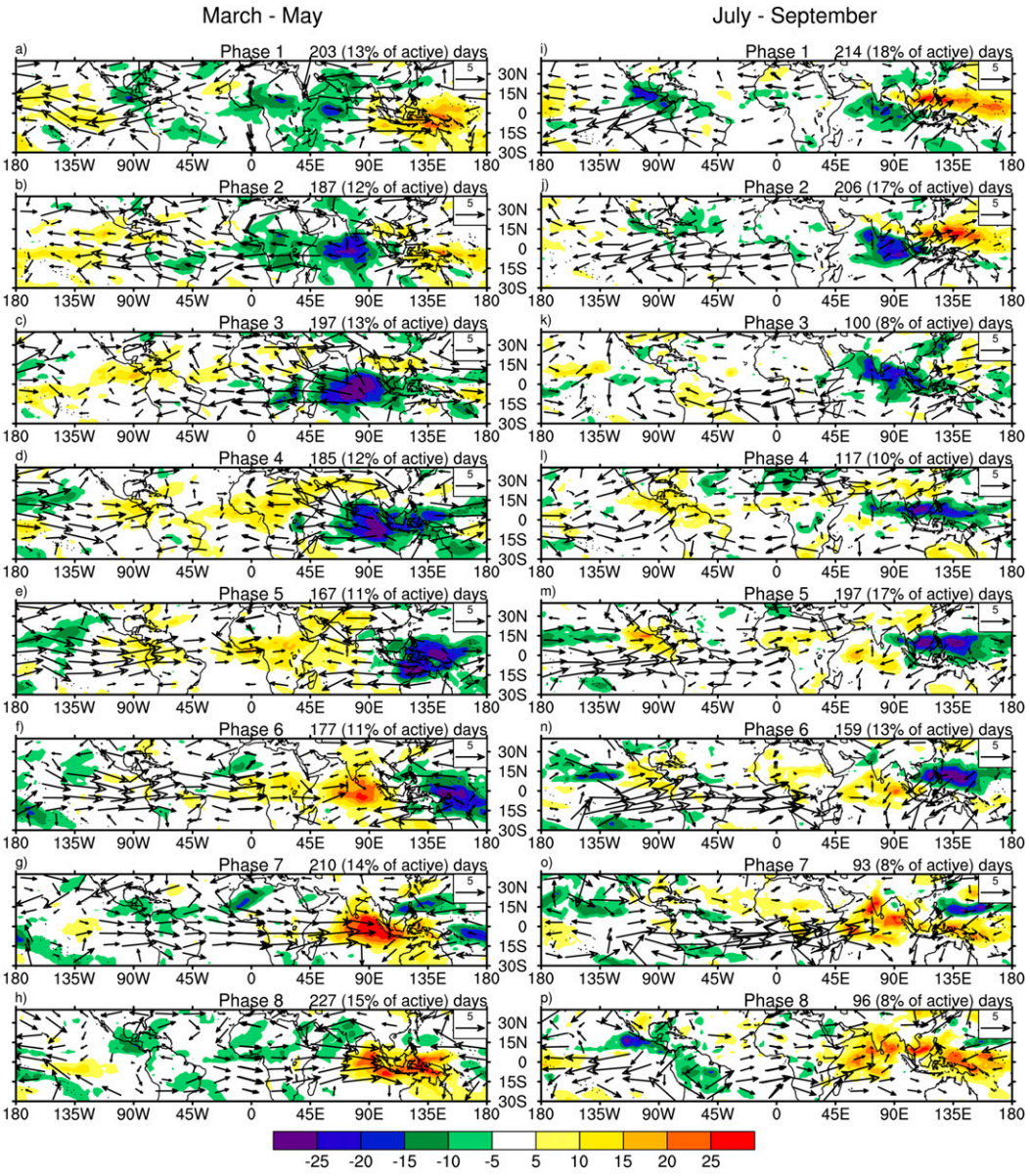

FIG. 2. Composites of anomalous OLR ($W\,m^{-2}$) and 200-hPa wind for phases of MJO (explained in text): (left) MAM and (right) JAS. Anomalies are computed as average for all days in stated phase minus average for all days defined as inactive. Reference wind vector ($m\,s^{-1}$) is shown in the top-right corner. Wind vectors are given at every 12th and 30th grid point plotted in latitude and longitude, respectively; those with magnitudes less than $1\,m\,s^{-1}$ are omitted. Number of (and percent of active) days in each phase is indicated in the top-right corner.

any precipitation. Therefore, for the subsequent analyses, the northern limit of the MAM domain will be set to 15°N.

We recognize a certain ambiguity in our choice of threshold for heavy events. In areas with many days of zero rainfall, events exceeding the 90th-percentile value may not be exceptional compared to the other rainy days. To assess the possible impact of including days with no precipitation in the threshold definition, Fig. 3b shows the value of the MAM 90th percentile computed excluding zero-rainfall days, and Fig. 3c shows the difference relative to the original percentile. The difference is less than 4 mm over most of the domain and is only large (>10 mm) in a small area near the west coast. So, for MAM at least, the inclusion of zero-rainfall days does not greatly affect the estimates of heavy-rainfall events.

Including zeros when computing the 90th percentile may be somewhat more of an issue in JAS. In contrast with MAM, the JAS threshold (Fig. 3d) varies substantially

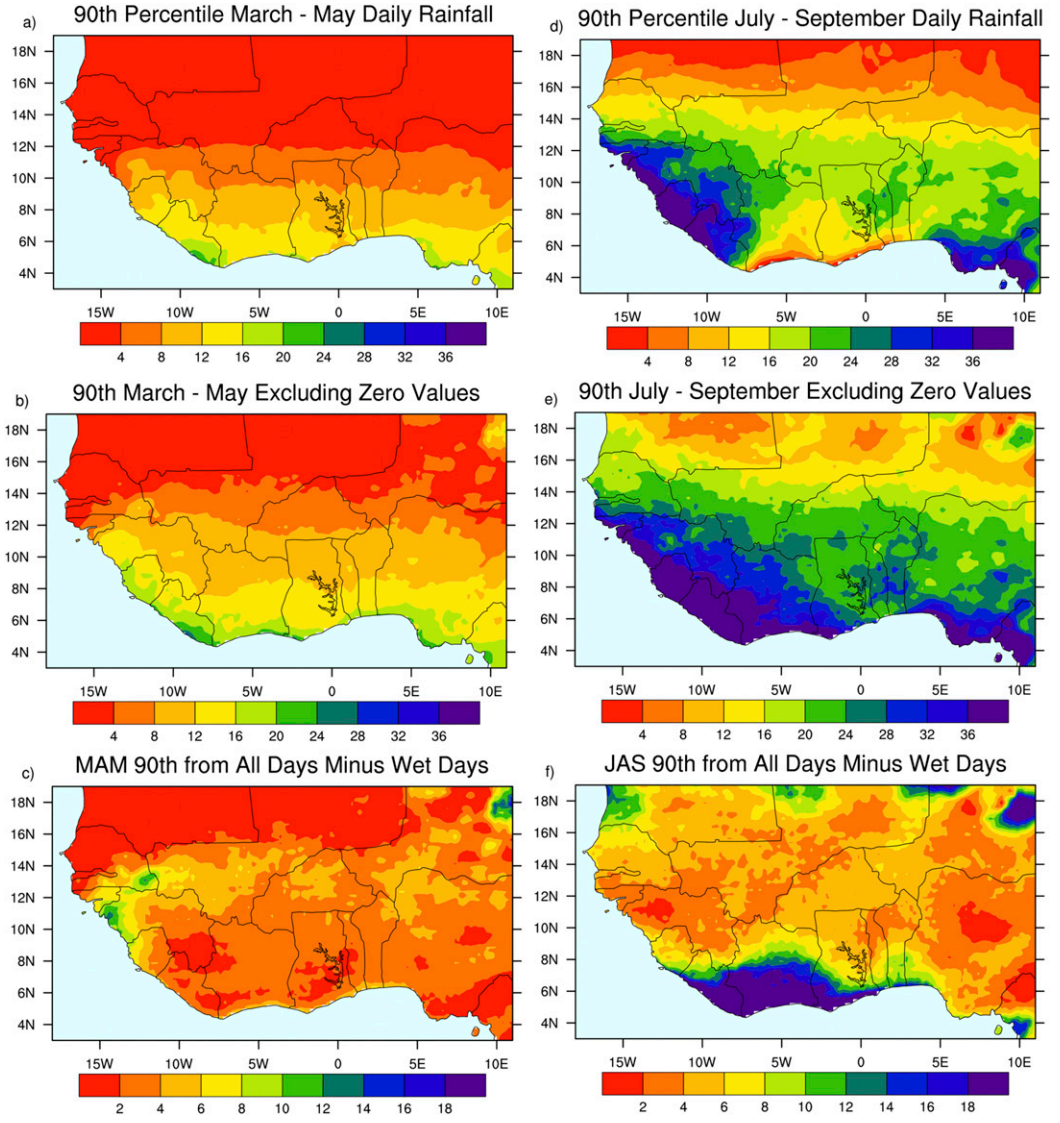

FIG. 3. The (a) 90th percentile of daily CHIRPS precipitation (mm) for all days in MAM; (b) 90th percentile of daily CHIRPS precipitation (mm) for days with precipitation in MAM; and (c) 90th percentile of daily CHIRPS precipitation (mm) for days with precipitation minus percentile for all days [i.e., difference between (a) and (b)]. (d)–(f) As in (a)–(c), but for JAS.

across southern West Africa, from large values along the southwest coast to quite low amounts farther east (near 0°) that are lower than in MAM. In that coastal region extending from the Ivory Coast into Benin, however, there are few JAS rainy days, but rainy day amounts are substantial. This leads to large differences between percentiles computed with and without days with zero rainfall (Fig. 3f). In particular, the reversal in the north–south gradient between 1°E and 8°W disappears when zero-rainfall days are excluded (cf. Figs. 3d,e). The statistical tests we apply later to establish whether the impact of the MJO is significant depend on there being the same number of extremes at each grid point; thus, an all-day 90th percentile is preferred. We will, however, reexamine our definition of "heavy event" when interpreting the results and show that the central findings of this study are not sensitive to this choice.

Having defined a spatially varying threshold for heavy daily precipitation events (albeit imperfect), we then ascertain which grid points exhibit a statistically significant increased or decreased frequency of such events coincident with a given MJO phase. For MAM, this local level of significance is determined empirically by drawing 1 000 000 random samples, each with a length of 167 days (which is the sampling size of the least sampled phase in MAM, phase 5), from a time series of length 3128 days (the total number of days per season for the

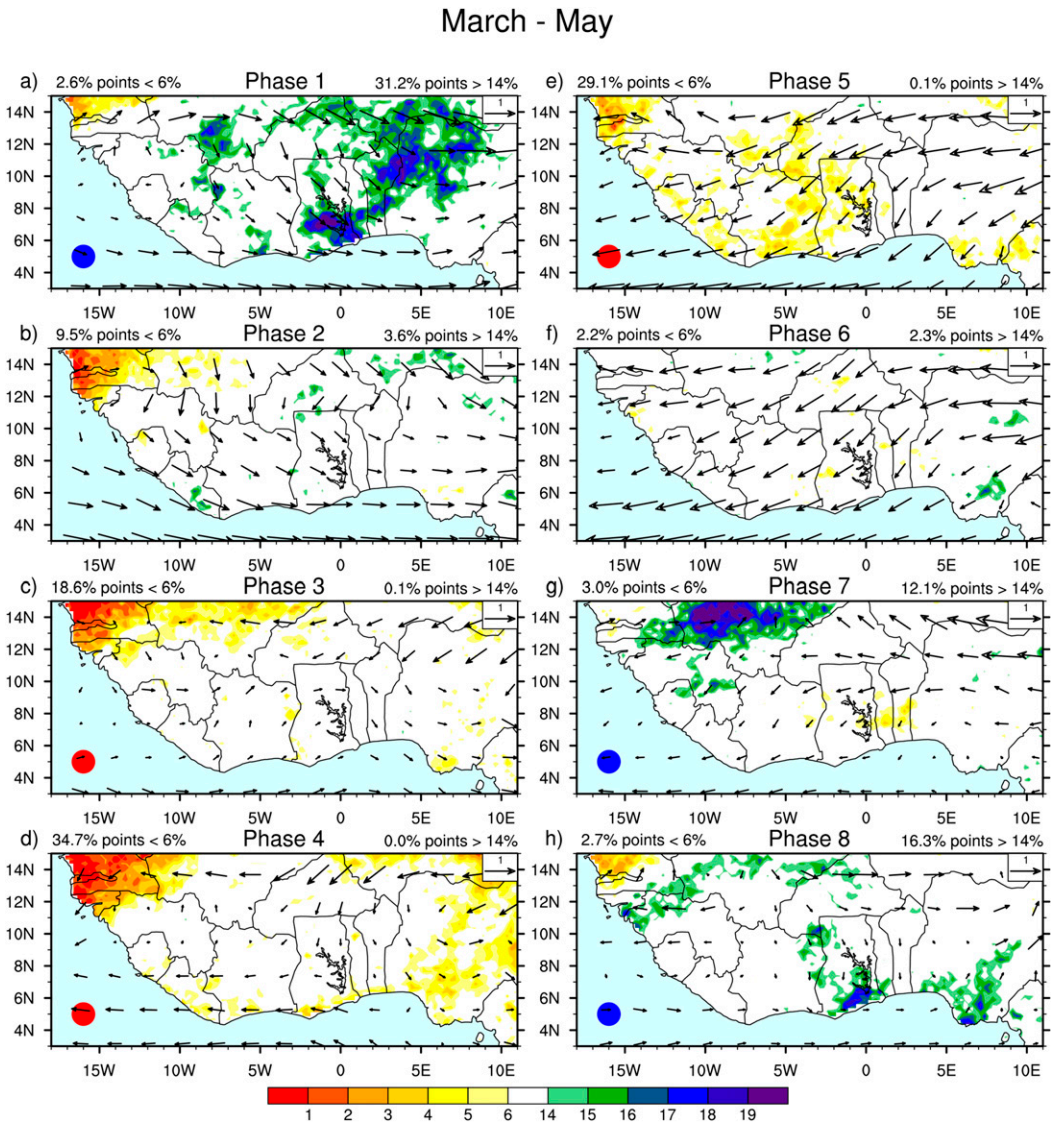

FIG. 4. Percent of heavy precipitation events (see text for definition) in each phase of MJO during MAM compared to total number of days in that phase. The percentages of grid points within the (land) domain with fewer than 6% or more than 14% heavy events (the chosen local significance levels) are shown in the top-left and top-right, respectively, of each map. Note uneven shading intervals. Wind vectors ($m\,s^{-1}$), which are plotted at every third grid point, show 850-hPa wind anomalies (phase indicated minus inactive). Reference vector (shown in top-right-hand corner of individual plots) is $1\,m\,s^{-1}$. Dots in the bottom-left corner of each map indicate field significance (see text for explanation) for increased (blue) and decreased (red) frequency of heavy events.

period 1981–2014). We then compute the percentage of heavy daily events (defined as exceeding the value of the 90th percentile in the complete time series) in each random sample and build the corresponding distribution. Note that, because of the definition of "heavy," the nature of the actual time series used is irrelevant. Using this test and this sample size, we find that a percentage value of 14% of heavy events corresponds to the 96th percentile in the random subset distribution. Thus, if the fraction of heavy events at a certain grid point during a particular MJO phase is higher than 14%, we can reject the null hypothesis (that the MJO does not affect the frequency of heavy events) with 96% confidence. For a larger sample size of 227 (MAM phase 8 with the most days), the 14% value represents an even higher confidence level (97%). For suppressed heavy events, we choose a 6% threshold, which is somewhat more significant than a 96% confidence level in all cases, again based on Monte Carlo tests.

Figure 4 shows the fraction of heavy daily precipitation events that occur in each subset of days corresponding

to a given MJO phase, relative to the total number of sample days in that phase, for MAM. Only percentages higher than 14% (green–blue shading) or lower than 6% (yellow–red shading) are plotted. During phase 1 (Fig. 4a), there is a swath from central to eastern West Africa over which heavy precipitation events occur on more than 14% of days, consistent with the mean rainy conditions implied by the composite negative OLR anomalies (Fig. 2a). As the main MJO convective center moves into the central Indian Ocean and negative OLR anomalies dwindle over West Africa (phase 2, Fig. 2b), the frequency of occurrence of heavy events in that region returns to near climatology. The subsequent dry phases (3–5) display an elevated number of grid points with reduced frequency of heavy events, as one would expect from the mean suppressed convection conditions, particularly phase 4 (Figs. 2d, 4d). As negative OLR anomalies return to the area (phases 7–8), the area exhibiting more than 14% of days with heavy events increases again, although in phase 7 this increase, which lines up well with negative OLR anomalies (Figs. 4g, 2g), is the result of modest precipitation amounts, since the 90th-percentile threshold there is small (Fig. 3a).

In addition to local significance, however, we also need to consider field significance. Indeed, even if precipitation were randomly distributed, there would still be a certain percentage of grid points at which the frequency of days with heavy precipitation in a given MJO phase would be locally significant (for instance, we expect about 4% of grid points to exceed the 96% significance level just by chance). One must then determine the percentage of grid points that needs to be locally significant in order for the field to be considered unlikely to occur by chance (Livezey and Chen 1983, hereafter LC83). Additionally, as pointed out by LC83, one must take into account the spatial autocorrelation, which reduces the number of degrees of freedom and, if not accounted for, spuriously increases the likelihood that a field will be considered significant.

The field significance test used here also employs randomization, following LC83. For each phase and season, a million random fields of length N_P are drawn from the original seasonal daily precipitation dataset, where N_P is the number of days in that MJO phase for that season. This procedure preserves the autocorrelation in the field. Local significance is then assessed in the same way as for the actual MJO subset of days, the fraction of grid points meeting this local criterion is computed, and the corresponding random distribution is built. If the actual observed fraction of locally significant points lies outside the 2.5%–97.5% percentile range of the random distribution, that observed MJO field is considered to be statistically significant at the 5% confidence level. In Figs. 4 and 5, significant fields are indicated by a blue or red dot in the lower-left corner. The proportion of grid points with a significant excess or deficit of heavy events is also displayed at the top of each panel.

The increase in heavy-rainfall events detected in phases 7, 8, and 1, as the MJO convection dies over the date line and the main MJO convective center redevelops over the Indian Ocean, are all field significant. So are the observed decreases in phases 3, 4, and 5, which correspond to locally dry MJO phases (Fig. 4). Enhanced and suppressed heavy events during phases 1 and 5, respectively, are in keeping with the results of Berhane et al. (2015), who showed a consistent MJO-related shift in the probability distribution of area-averaged daily rainfall in these two phases, although the area of interest extended farther east and south compared to the present study. The 850-hPa winds shown in Fig. 4 are also consistent with those in Berhane et al. (2015), with (weak) anomalous westerlies during times of enhanced rainfall events and anomalous easterlies during episodes when they are suppressed.

Figure 5 displays the same composite as Fig. 4, but for JAS (using the full domain and adjusting the sampling size in the randomized local significance tests). Like in MAM, phase 1 exhibits an above-normal frequency of heavy events, which is field significant (Fig. 5a), although now the largest increases are concentrated in the western Sahel. Unlike in MAM, JAS phase 2 also exhibits a field-significant increase in heavy-event frequency (Fig. 5b), with most of the signal occurring along the south coast of the Ivory Coast and Ghana. The association between the MJO and daily JAS rainfall, however, could be of a different nature in these two phases and regions, given our choice of threshold (the 90th percentile for all days) and the contrasting seasonal precipitation regimes: that is, the Sahel is wet compared to MAM while the coast is dry, both in terms of mean precipitation (Figs. 1b,c) and the 90th percentile (Figs. 3a,d).

This qualitative difference in MJO impact can be seen by constructing histograms, stratified by MJO phase, of anomalous counts of grid point per days (relative to the corresponding average number in all active and inactive phases) in four precipitation categories, for the northern and southern regions outlined in Figs. 5a and 5b. These histograms are presented in Fig. 6a for the northern Sahel region (at the border of Mauritania, Senegal, and Mali) and Fig. 6b for the southern coastal region (which stretches across Ghana and the Ivory Coast). The 90th percentile for all days and rainy days only, for each region as a whole, is also shown (vertical lines). For both the northern region during phase 1 and the southern region during phase 2, there is a pronounced decrease in

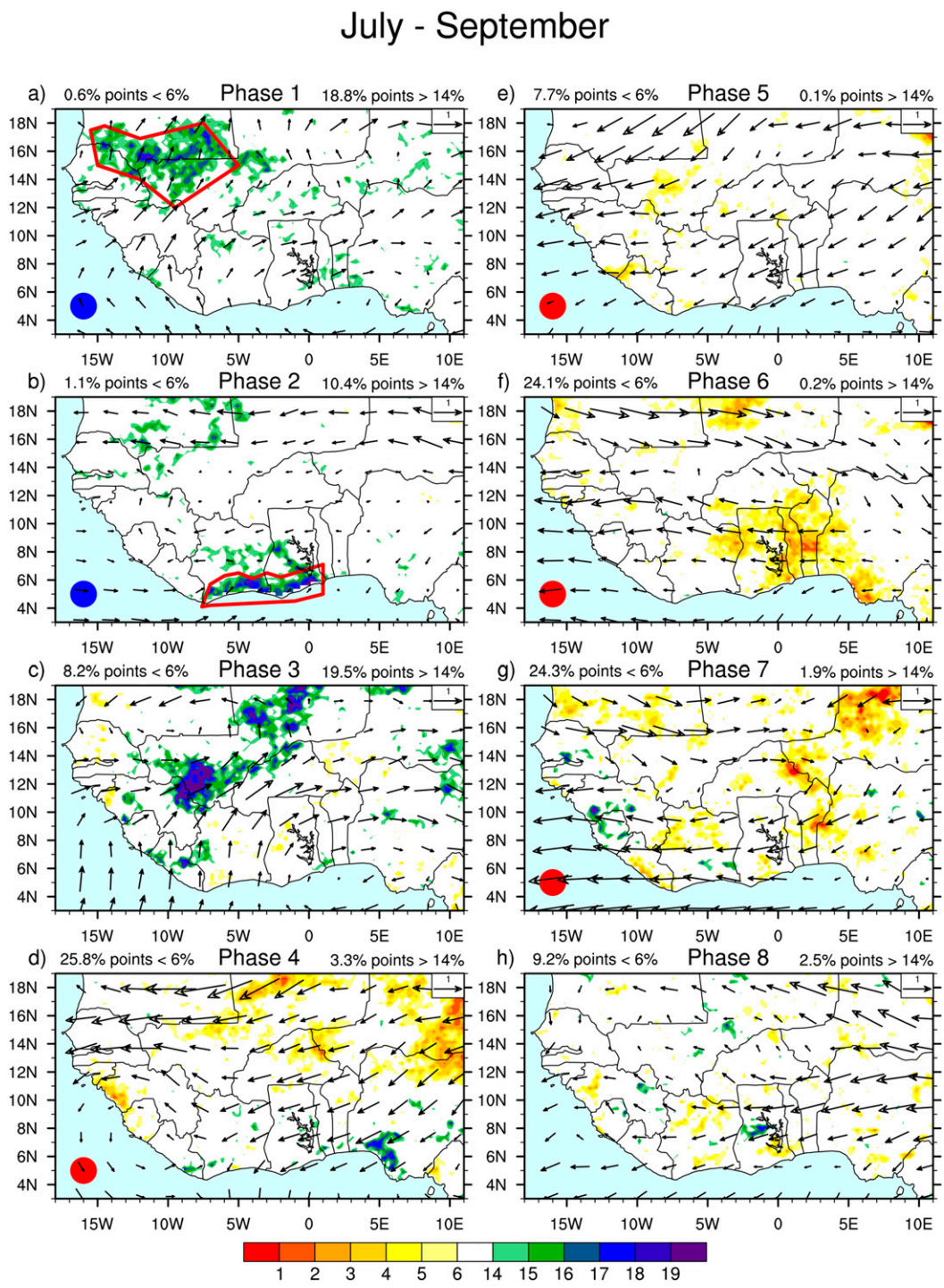

FIG. 5. As in Fig. 4, but for JAS. In (a),(b), polygons show regions selected for the histograms in Fig. 6.

daily events with <1 mm rainfall, with a compensating increase in all the other categories. For the Sahel region, however, the largest increase, especially in relation to the baseline across all phases (including inactive), occurs for events exceeding the 90th percentile for rainy days (red line), implying more frequent heavy-rainfall days during the locally wet monsoon season. Instead, for the southern region, which is experiencing its dry season, the increase in heavy events (as defined by the all-day 90th percentile; purple line) actually reflects an increase in

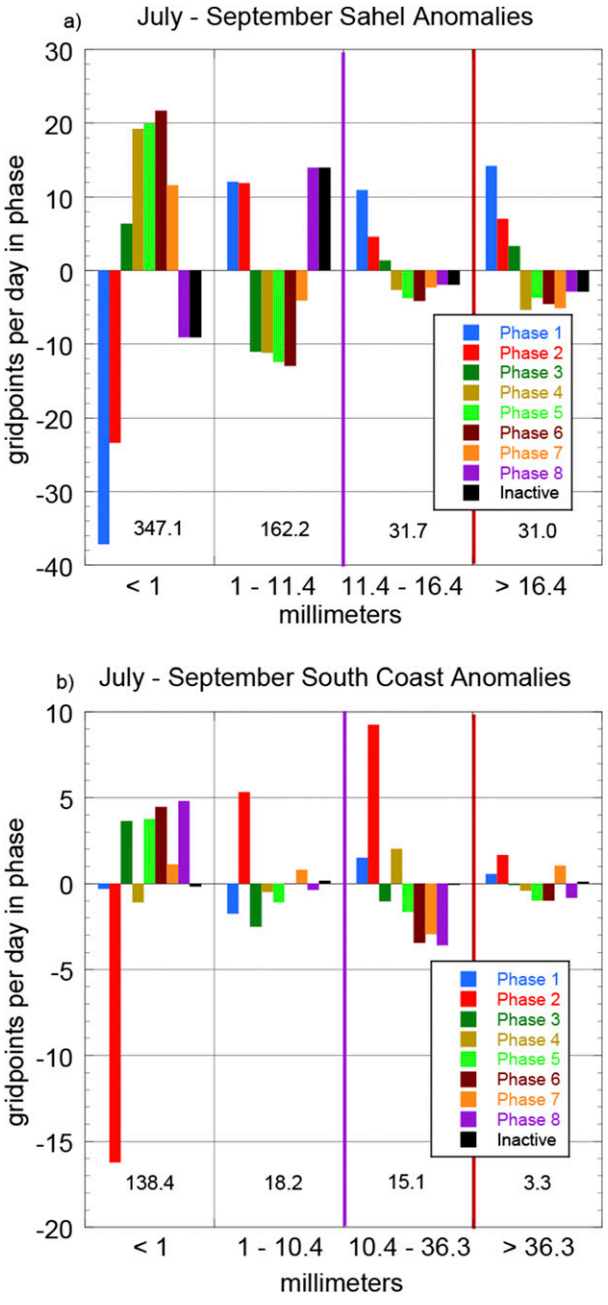

FIG. 6. Histograms of anomalous counts of grid points per day for different categories of daily precipitation amounts (mm; range stated on *x* axis), in each MJO phase and in inactive phase, for the season and region indicated in the title. (a),(b) The regions shown in Figs. 5a and 5b, respectively. The vertical purple (dark red) line denotes the 90th-percentile limit determined from all grid points and all days (days with nonzero rainfall). The counts are expressed as anomalies of number of grid points per day relative to the average over all phases, including inactive (indicated near the bottom of each bin).

days with modest precipitation, while the truly heavy-rainfall events (exceeding the much higher rainy-day 90th percentile) increase only slightly. Thus it appears that, in JAS, the early stages of the MJO increase the risk of flooding in Mauritania, Senegal, and Mali (phase 1) but provide drought relief to the Ivory Coast and Ghana (phase 2).

Phase 3 (Fig. 5c) in JAS has a larger count of grid points with locally significant increases in heavy events than phase 1, but this signal is not field significant, as there are relatively few (100) days in that phase. Nevertheless, this result is again in contrast with its MAM counterpart (Fig. 4c), which has significantly fewer heavy events than expected. The next four phases (Figs. 5d–g) show field-significant reductions in heavy precipitation, an effect that is also present in MAM but limited to phases 4 and 5 (Figs. 4d,e). In fact, the extended suppression of precipitation during the passage of the MJO up until phase 7 (Fig. 5g) constitutes another difference with MAM, for which the same phase exhibits a field-significant increase in heavy daily rainfall (Fig. 4g).

4. Summary and conclusions

We have examined the influence of the MJO on West Africa precipitation during MAM, a wet season in southern West Africa, and JAS, the peak wet season in most of the domain (except the southcentral coast), with emphasis on the largest daily events. A heavy event was defined subjectively to be rainfall in the top 10% of daily events at each 0.25° × 0.25° grid point (the results are qualitatively similar if this percentile is changed). The MJO phases were determined from the RMM index developed by Wheeler and Hendon (2004). Local and field statistical significance were determined by randomization methodologies.

The relative counts, or fraction, of daily heavy events stratified by MJO phase indicate a strong and statistically robust enhancement (suppression) during certain MJO phases characterized by convection (subsidence) in the area. The results from the two seasons are broadly similar in that phase 1 shows an increased frequency of occurrence of heavy events in both MAM and JAS, while phases 4 and 5 show a significant reduction. There are also, however, substantial differences between the seasons. For example, phase 7 shows field-significant increases in extremes in MAM but field-significant decreases in JAS (Figs. 4g, 5g). One may have expected the MJO impact on heavy events to be weaker in JAS than MAM because MJO-related OLR anomalies are weaker [e.g., Fig. 2 and Berhane et al. (2015)]. Yet we find comparable changes in both seasons in terms of number of phases with field significance, even though

the amount needed for a daily event to qualify as heavy is generally larger in JAS (Fig. 3). This is in contrast with Berhane et al. (2015), who found slightly enhanced and substantially reduced daily rainfall amounts over equatorial West Africa during active and suppressed phases, respectively, in March–June, but no change in extremes in JAS. The discrepancies are likely due to differences in analysis techniques. The results are somewhat sensitive to the threshold used to differentiate active and inactive phases. If the threshold is set high (e.g., an MJO amplitude above 2), the number of days in each category decreases, so a larger number of grid points with a locally significant increase in heavy events is required in order to achieve field significance. If the threshold is set low (e.g., an MJO amplitude less than 1), the area with significant changes increases, but the actual changes in extreme count are modest. Our subjectively chosen amplitude of 1.25 attempts to balance significance with relevance.

Although we have broadly examined the influence of the MJO on the tail of the distribution, the actual nature of this impact depends on the specific local and seasonal precipitation regime. For instance, in JAS, when the ITCZ moves northward, wetting the Sahel but leaving the southern coast dry (Fig. 1c), the increase in heavy events in the Sahel during phase 1 and in the southern coast during phase 2 has widely different practical consequences (Figs. 5a,b). In the former case, such an increase truly reflects more frequent episodes of heavy precipitation and increased risk of flooding during the local wet monsoon season (Fig. 6a). In the latter case, the result is best viewed as a decrease in the number of dry days and thus a welcome relief during the dry season.

Histograms for individual regions and for the entire domain (not shown) indicate that, in both seasons, a significant increase (decrease) in heavy precipitation events associated with a given MJO phase is generally accompanied by a decrease (increase) in the number of near-zero-rainfall days, balanced by an opposite change across all rainy categories. Although this is hardly surprising, it suggests a role for the background state associated with the MJO in providing an environment more or less conducive to convection, depending on its sign. We have not, however, addressed the issue of the dynamical links between the large-scale MJO circulation and cloud cover and the local heavy-rainfall events. Again, these links must depend on the local dynamical regime in a particular season and also on the type of rain-producing mesoscale convective systems most prevalent in each region. For instance, squall lines in the Sahel during the monsoon season (Gaye et al. 2005) may be favored in phase 1 by MJO-induced vertical redistribution of moisture or changes in vertical shear or stability. Although it would be interesting to quantify the MJO modulation of convective available potential energy (CAPE), moist static energy, or moisture flux convergence in each phase, region, and season, such an in-depth analysis is outside the scope of this work.

In conclusion, by making conservative assumptions, this study has shown that the MJO modulates the occurrence of heavy daily precipitation events in West Africa during certain phases, in both MAM and JAS. Therefore, with further development, one may be able to issue probabilistic forecasts of heavy precipitation based on forecasts of the MJO.

Acknowledgments. We thank all the reviewers for exceptionally fair and insightful reviews. In particular, the detailed suggestions provided by reviewers 2 and 3 forced us to understand many subtleties that had been swept under the rug. AS was supported by the Significant Opportunities in Atmospheric Research and Science (SOARS) program, NSF Grant AGS-1120459, with additional funding provided by the NOAA Climate Program Office, Grant NA11NWS4620014. BL and DA were funded by United States Agency for International Development, FEWSNET NA150AR4320137. IB was funded by COMETH CGL 2012-30641 of the Spanish MICINN.

REFERENCES

Annamalai, H., and J. M. Slingo, 2001: Active/break cycles: Diagnosis of the intraseasonal variability of the Asian summer monsoon. *Climate Dyn.*, **18**, 85–102, doi:10.1007/s003820100161.

Berhane, F., B. Zaitchik, and H. S. Badr, 2015: The Madden–Julian oscillation's influence on spring rainy season precipitation over equatorial West Africa. *J. Climate*, **28**, 8653–8622, doi:10.1175/JCLI-D-14-00510.1.

ECMWF, 2009: ERA-Interim project. Research data archive at the National Center for Atmospheric Research, Computational and Information Systems Laboratory, accessed 6 February 2015, doi:10.5065/D6CR5RD9.

Funk, C. C., and Coauthors, 2014: A quasi-global precipitation time series for drought monitoring. U.S. Geological Survey Data Series 832, 4 pp., doi:10.3133/ds832.

——, A. Verdin, J. Michaelsen, P. Peterson, D. Pedreros, and G. Husak, 2015: A global satellite-assisted precipitation climatology. *Earth Syst. Sci. Data*, **7**, 275–287, doi:10.5194/essd-7-275-2015.

Gaye, A., A. Viltard, and P. de Felice, 2005: Squall lines and rainfall over western Africa during summer 1986 and 1987. *Meteor. Atmos. Phys.*, **90**, 215–224, doi:10.1007/s00703-005-0116-0.

Gu, G., 2009: Intraseasonal variability in the equatorial Atlantic–West Africa during March–June. *Climate Dyn.*, **32**, 457–471, doi:10.1007/s00382-008-0428-0.

Hagos, S. M., and K. H. Cook, 2007: Dynamics of the West African monsoon jump. *J. Climate*, **20**, 5264–5284, doi:10.1175/2007JCLI1533.1.

Hendon, H. H., and M. L. Salby, 1994: The life cycle of the Madden–Julian oscillation. *J. Atmos. Sci.*, **51**, 2225–2237, doi:10.1175/1520-0469(1994)051<2225:TLCOTM>2.0.CO;2.

Huffman, G. J., and D. T. Bolvin, 2013: GPCP version 2.2 SG combined precipitation data set documentation. NASA, 46 pp. [Available online at ftp://precip.gsfc.nasa.gov/pub/gpcp-v2.2/doc/V2.2_doc.pdf.]

Janicot, S., F. Mounier, N. M. J. Hall, S. Leroux, B. Sultan, and G. N. Kiladis, 2009: The dynamics of the West African monsoon. Part IV: Analysis of the 25–90-day variability of convection and the role of the Indian monsoon. *J. Climate*, **22**, 1541–1565, doi:10.1175/2008JCLI2314.1.

Jones, C., L. M. V. Carvalho, R. W. Higgins, D. E. Waliser, and J.-K. E. Schemm, 2004a: A statistical forecast model of tropical intraseasonal convective anomalies. *J. Climate*, **17**, 2078–2095, doi:10.1175/1520-0442(2004)017,2078:ASFMOT.2.0.CO;2.

——, D. E. Waliser, K. M. Lau, and W. Stern, 2004b: Global occurrences of extreme precipitation and the Madden–Julian oscillation: Observations and predictability. *J. Climate*, **17**, 4575–4589, doi:10.1175/3238.1.

——, A. Hazra, and L. M. V. Carvalho, 2015: The Madden–Julian oscillation and boreal winter forecast skill: An analysis of NCEP CFSv2 reforecasts. *J. Climate*, **28**, 6297–6307, doi:10.1175/JCLI-D-15-0149.1.

Kiladis, G. N., J. Dias, K. H. Straub, M. C. Wheeler, S. N. Tulich, K. Kikuchi, K. M. Weickmann, and M. J. Ventrice, 2014: A comparison of OLR and circulation-based indices for tracking the MJO. *Mon. Wea. Rev.*, **142**, 1697–1715, doi:10.1175/MWR-D-13-00301.1.

Knutson, T. R., and K. M. Weickmann, 1987: 30–60-day atmospheric oscillations: Composite life cycles of convection and circulation anomalies. *Mon. Wea. Rev.*, **115**, 1407–1436, doi:10.1175/1520-0493(1987)115<1407:DAOCLC>2.0.CO;2.

Lau, W. K.-M., D. E. Waliser, A. J. Majda, and S. N. Stechamnn, 2012: Multiscale theories for the MJO. *Intraseasonal Variability in the Atmosphere–Ocean Climate System*, W. K.-M. Lau and D. E. Waliser, Eds., Springer Berlin Heidelberg, 549–568, doi:10.1007/978-3-642-13914-7_17.

Le Barbé, L., T. Lebel, and D. Tapsoba, 2002: Rainfall variability in West Africa during the years 1950–90. *J. Climate*, **15**, 187–202, doi:10.1175/1520-0442(2002)015<0187:RVIWAD>2.0.CO;2.

Livezey, R. E., and W. Y. Chen, 1983: Statistical field significance and its determination by Monte Carlo techniques. *Mon. Wea. Rev.*, **111**, 46–59, doi:10.1175/1520-0493(1983)111<0046:SFSAID>2.0.CO;2.

Madden, R. A., and P. R. Julian, 1971: Detection of a 40–50 day oscillation in the zonal wind in the tropical Pacific. *J. Atmos. Sci.*, **28**, 702–708, doi:10.1175/1520-0469(1971)028<0702:DOADOI>2.0.CO;2.

——, and ——, 1972: Description of global-scale circulation cells in the tropics with a 40–50 day period. *J. Atmos. Sci.*, **29**, 1109–1123, doi:10.1175/1520-0469(1972)029<1109:DOGSCC>2.0.CO;2.

——, and ——, 1994: Observations of the 40–50-day tropical oscillation—A review. *Mon. Wea. Rev.*, **122**, 814–837, doi:10.1175/1520-0493(1994)122<0814:OOTDTO>2.0.CO;2.

Maloney, E. D., and J. Shaman, 2008: Intraseasonal variability of the West African monsoon and Atlantic ITCZ. *J. Climate*, **21**, 2898–2918, doi:10.1175/2007JCLI1999.1.

Matthews, A. J., 2004: Intraseasonal variability over tropical Africa during northern summer. *J. Climate*, **17**, 2427–2440, doi:10.1175/1520-0442(2004)017<2427:IVOTAD>2.0.CO;2.

Pohl, B., S. Janicot, B. Fontaine, and R. Marteau, 2009: Implication of the Madden–Julian oscillation in the 40-day variability of the West African monsoon. *J. Climate*, **22**, 3769–3785, doi:10.1175/2009JCLI2805.1.

Pu, B., and K. H. Cook, 2010: Dynamics of the West African westerly jet. *J. Climate*, **23**, 6263–6276, doi:10.1175/2010JCLI3648.1.

Rodríguez-Fonseca, B., and Coauthors, 2015: Variability and predictability of West African droughts: A review on the role of sea surface temperature anomalies. *J. Climate*, **28**, 4034–4060, doi:10.1175/JCLI-D-14-00130.1.

Straub, K. H., 2013: MJO initiation in the real-time multivariate MJO index. *J. Climate*, **26**, 1130–1151, doi:10.1175/JCLI-D-12-00074.1.

Sultan, B., and S. Janicot, 2000: Abrupt shift of the ITCZ over West Africa and intra-seasonal variability. *Geophys. Res. Lett.*, **27**, 3353–3356, doi:10.1029/1999GL011285.

——, and ——, 2003: The West African monsoon dynamics. Part II: The ''preonset'' and ''onset'' of the summer monsoon. *J. Climate*, **16**, 3407–3427, doi:10.1175/1520-0442(2003)016<3407:TWAMDP>2.0.CO;2.

Wheeler, M. C., and H. H. Hendon, 2004: An all-season real-time multivariate MJO index: Development of an index for monitoring and prediction. *Mon. Wea. Rev.*, **132**, 1917–1932, doi:10.1175/1520-0493(2004)132<1917:AARMMI>2.0.CO;2.